Analysis, Control, and Wireless Charging of Energy Systems Using Ultracapacitors

Chen Zhao, He Yin, Minfan Fu
University of Michigan-Shanghai Jiao Tong
University Joint Institute,
Shanghai Jiao Tong University,
Shanghai, P. R. China
Email: chenzhaosjtu@gmail.com;
yyy@sjtu.edu.cn;
fuminfan@sjtu.edu.cn

Chengbin Ma*[1,2]
1. University of Michigan-Shanghai Jiao Tong
University Joint Institute;
2. School of Mechanical Engineering,
Shanghai Jiao Tong University,
Shanghai, P. R. China
Email: chbma@sjtu.edu.cn

***Abstract*—The battery-ultracapacitor hybrid energy storage system (HESS) and its management have been widely investigated in recent years. Meanwhile, there is a lack of general and quantitative analysis on the energy loss of the battery-ultracapacitor HESS that does not depend on any specific control algorithm or physical limitations. In addition, the battery-ultracapacitor HESS is actually a simple example of a networked energy system. An agent-based control approach is desirable in order to improve the synergy, and thus, the flexibility, scalability, fault-tolerance and reliability of the hybrid energy systems, and also the computational efficiency. Finally, considering the requirement of fast and frequent wireless charging, ultracapacitors could be more suitable than batteries due to their excellent reliability and charge/discharge capability. In this paper, these three aspects for the energy systems using ultracapacitors, i.e., analysis, control, and wireless charging, are discussed.**

***Index Terms*—Ultracapacitor, Hybrid energy storage system, Efficiency, Optimized Control, Wireless Charging**

I. Introduction

Currently, batteries are one of the most commonly used energy storage devices. However, their energy and power densities, reliability, cycle-life and management are always problematic. Batteries alone often cannot meet load requirements efficiently and continuously. In recent years, the battery-ultracapacitor hybrid energy storage system (HESS) and its management have been widely investigated. The basic idea is to use ultracapacitors (UCs) as an assistant energy storage device for improving the efficiency, reliability, and dynamic response of the overall HESS [1], [2]. This also avoids the necessity of an oversized battery pack due to the power requirement [3], [4].

The primary disadvantage of UCs is their relatively low energy density compared to batteries [5]. Thus hybridization of batteries and UCs provides high energy density, long cycle life, and low cost. It is considered to be the best usage of UCs in real applications [5], [6]. Various configurations of the HESS are possible with different number and placement of the DC-DC converters [7]. In order to improve system energy efficiency and life expectancy of batteries, many energy management strategies have also been proposed such as an optimal-control-model approach [8], a wavelet-transform-based algorithm [9], rule-based and fuzzy logic approaches [10]–[12], model predictive control [12], a probability-weighted Markov process [13], and a multi-objective optimization approach [14].

Meanwhile, 1) there is a lack of general and quantitative analysis on the energy loss of the battery-ultracapacitor HESS that does not depend on any specific control algorithm or physical limitations. This analysis is important to establish guidelines for evaluation and improvement purposes. 2) the battery-ultracapacitor HESS is relatively simple, but still an example of a networked energy system. An agent-based control approach is desirable in order to improve the synergy, flexibility, scalability, fault-tolerance and reliability of the hybrid energy systems, and the computational efficiency. 3) wireless power transfer (WPT) not only provides an easier and safer experience of high voltage and high current daily charging process, but also enables a totally new direction of management of electrical power efficiently. Especially it provides an alternative solution without requiring dramatic improvements in battery technology [15], [16]. Considering the requirement of fast and frequent wireless charging, ultracapacitors could be more suitable than batteries due to their excellent reliability and charge/discharge capability. Based on the above basic considerations, these three aspects, i.e., analysis, control, and wireless charging, are discussed in the following sections.

II. Topology and Experimental Setup

Using a single DC-DC converter, two semi-active topologies are possible for the battery-ultracapacitor HESS, i.e., capacitor semi-active and battery semi-active hybrids [7]. In the battery semi-active hybrid, the DC-DC converter is placed between the battery pack and the load, as shown in Fig. 1. The battery semi-active hybrid is capable of enforcing the battery to work at the point close to the average power/current, therefore reducing the power rating of the DC-DC converter, prolonging cycle-life of the battery pack, and improving energy efficiency [4], [7], [17]. Figure 2 shows the experimental setup of the battery-ultracapacitor HESS, which employs the battery semi-active topology. The power supply and the electronic load

978-1-4799-6075-0/14/$31.00

are controlled to emulate charging and discharging currents, respectively. The boost DC-DC converter is designed and fabricated in house with an overall efficiency being more than 90%.

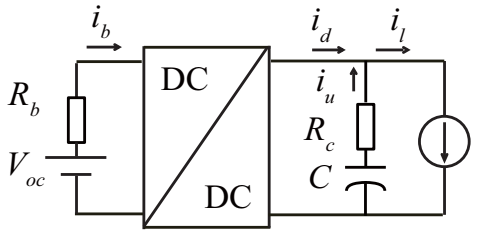

Fig. 1. The topology of the battery semi-active HESS.

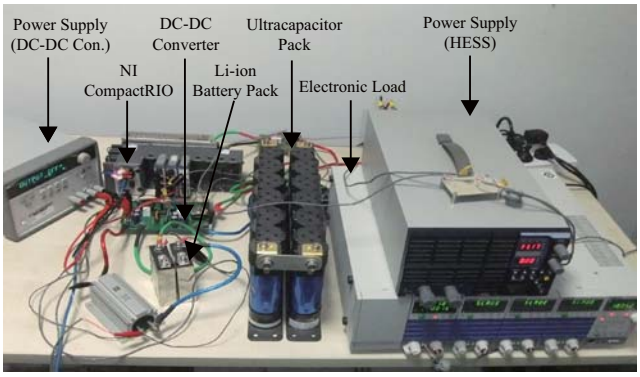

Fig. 2. Experimental battery semi-active HESS.

III. ESR-BASED EFFICIENCY ANALYSIS

As shown in Fig. 3, the overall power loss P_{loss} of the battery semi-active HESS can be represented as

$$P_{loss} = i_d^2(R_b^* + R_d^*) + i_u^2 R_u^*, \tag{1}$$

where "*" denotes an equivalent series resistance (ESR) in terms of energy loss. i_d is the output current of the DC-DC converter. i_u is the UC current. R_b^*, R_d^*, and R_u^* are the ESRs for the battery pack, the DC-DC converter, and the UC pack, respectively.

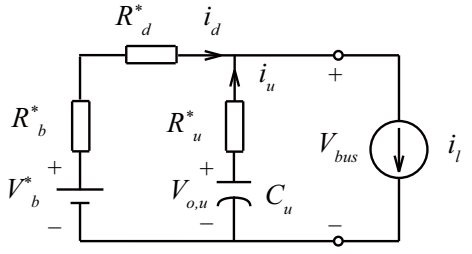

Fig. 3. ESR circuit for the battery semi-active HESS.

The ESR of the DC-DC converter can be derived using its first-order model,

$$\begin{aligned} R_d^* &= \frac{P_{loss,d}}{i_d^2} \\ &\approx \frac{R_L + d_s R_{MOS}}{(1-d_s)^2} + R_{D1} + \frac{V_F}{i_d} \\ &= R_{d,r}^* + \frac{V_F}{i_d}, \end{aligned} \tag{2}$$

where $P_{loss,d}$ is the power loss in the DC-DC converter. d_s is the switching duty cycle. R_{MOS} is the on-resistance of the MOSFET switch. R_L is the ESR of the inductor L. The diode here is modeled as a series combination of a constant voltage source V_F and a resistance R_{D1}. Similarly, the ESRs for the battery and UC packs are

$$R_b^* \approx \frac{R_s}{(1-d_s)^2}, \tag{3}$$

$$R_u^* \approx R_{sc}, \tag{4}$$

where R_s and R_{sc} are the internal resistances for the battery and UC packs, respectively.

For a theoretical analysis, a pulsed current load profile is used here to represent the dynamic power requirement [7], [18]. The decomposition of the pulsed current load is illustrated in Fig. 4, where $I_{l,max}$ and $I_{l,min}$ are the maximum and minimum load currents, respectively. T is the period and D is the duty cycle of the pulsed current load. The pulsed load current i_l can be decomposed into two components, average current $I_{l,a}$ and dynamic current $i_{l,d}$. $I_{l,dp}$ and $I_{l,dn}$ are the dynamic current $I_{l,d}$ during DT and $(1-D)T$. Then based on Equ. (1)-(4),the energy loss of the battery semi-active HESS, E_{loss}, in period T can be calculated as

$$\begin{aligned} E_{loss} = &- I_{l,dp} I_{l,dn} (R_b^* + R_{d,r}^* + R_u^*) \left(C_d - \frac{1}{1+K} \right)^2 T \\ &- I_{l,dp} I_{l,dn} R_p^* T + I_{l,a}^2 (R_b^* + R_{d,r}^*) T + I_{l,a} V_F T, \end{aligned} \tag{5}$$

where K and R_p^* are defined as

$$K = \frac{R_b^* + R_{d,r}^*}{R_u^*}, \tag{6}$$

$$R_p^* = \frac{1}{\dfrac{1}{R_{d,r}^* + R_b^*} + \dfrac{1}{R_u^*}}. \tag{7}$$

Here a new parameter, C_d, is defined to represent the dynamic current distribution between the DC-DC converter (i.e, the battery pack) and the UC pack, namely

$$C_d \triangleq \frac{I_{d,d}}{I_{l,d}} = \frac{I_{d,max} - I_{l,a}}{I_{l,dp}} = \frac{I_{d,min} - I_{l,a}}{I_{l,dn}}. \tag{8}$$

$I_{d,d}$ is the dynamic current provided by the DC-DC convert (i.e., the battery pack). $I_{d,max}$ and $I_{d,min}$ are the dynamic current from the DC-DC converter in DT and $(1-D)T$, respectively. It is obvious that for a minimized overall energy

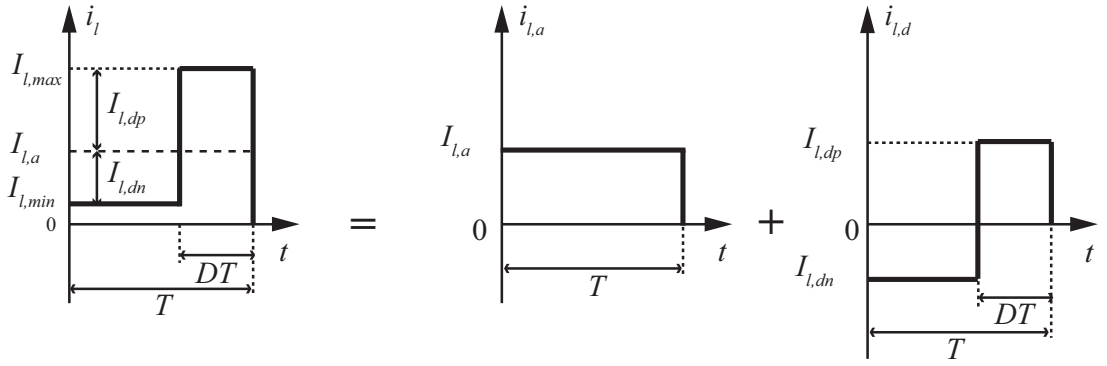

(a) The decomposition of pulsed load current

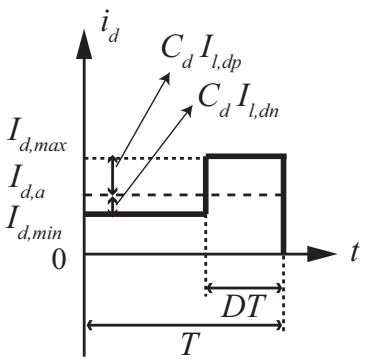

(b) Current from DC-DC converter

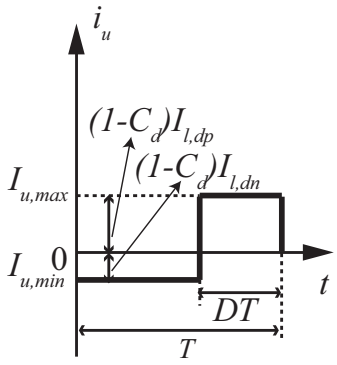

(c) Current from UC pack

Fig. 4. Dynamic current distribution during a single period.

loss, the optimal C_d^* is

$$C_d^* = \frac{1}{K+1}. \tag{9}$$

For the battery-ultracapacitor HESSs, usually the internal resistance of the battery pack is much larger than that of the UC pack, i.e., a close-to-zero C_d^*. This result is interesting because it theoretically proves that both the battery protection and the improvement on the system energy efficiency require the battery pack to provide an average current, and the UC pack mainly supplies the dynamic current. As shown in Fig. 5, the simulation and experimental results, the basic trend is larger the C_d, more the overall energy loss, E_{loss}, under a pulsed current load. However, the optimal C_d^* is actually not zero, but a small close-to-zero number (about 0.008 here). These results well match the previous theoretical analysis, and could serve as a base for discussing various real-time HESS control algorithms.

For reference purposes, the JC08 driving cycle is used here to represent a more realistic driving cycle. It is the new Japanese urban test cycle representing a congested city driving, in which the maximum speed is 81.6 km/h and the average speed is 24.4 km/h [see Fig. 6]. As shown in Fig. 7, similar results can be found between the overall energy loss and C_d, while the relationship deviates a little bit from the ideal quadratic relationship [refer to Eq. (5)]. However, the optimal

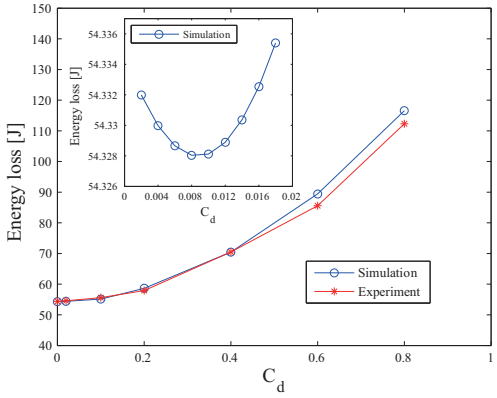

Fig. 5. Overall energy loss versus C_d under a pulsed current load.

C_d^* is still close to 0.008, which validates the above theoretical analysis.

IV. Utility Function-based Control

Although the battery-ultracapacitor HESS is relatively simple, it actually can be considered as an example of a networked energy storage system. Here a utility-function/agent-based approach is introduced that reflects different preferences of the battery and UC packs [19]. For example, the utility function

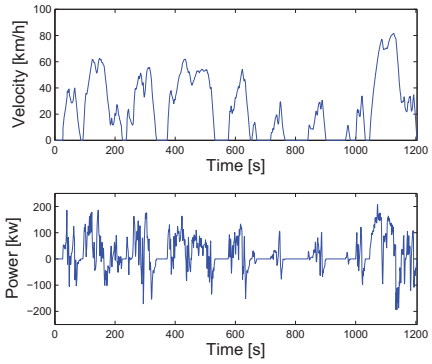

Fig. 6. JC08 velocity and power profiles.

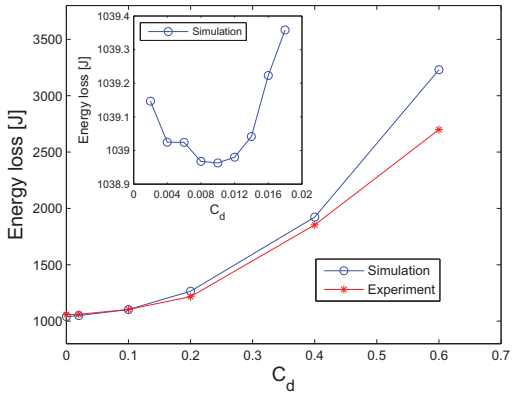

Fig. 7. Overall energy loss versus C_d under JC08 driving cycle.

of the battery pack, u_b, can be equivalent to the utility of the battery cycle-life:

$$u_b = w_{b,ave}u_{b,ave} + w_{b,dif}u_{b,dif}. \tag{10}$$

The aim of $u_{b,ave}$ is to minimize the amplitude of the battery current while the aim of $u_{b,dif}$ is to minimize the variation rate of the current. $w_{b,ave}$ and $w_{b,dif}$ are weight coefficients for $u_{b,ave}$ and $u_{b,dif}$, respectively. $u_{b,ave}$ and $u_{b,dif}$ are defined as

$$u_{b,ave} = 1 - a(i_b - i_{b,ave})^2, \tag{11}$$
$$u_{b,dif} = 1 - b(i_b - i_{b,l})^2, \tag{12}$$

respectively. Here $i_{b,ave}$ is the average current of the battery pack from the beginning to the current control instant. $i_{b,l}$ is the current of the battery pack at the last control instant. The coefficients, a and b, can be calculated using Eqs. (13)(14). The two equations are designed to normalize $u_{b,ave}$ and $u_{b,dif}$, respectively. The threshold, $Max(|i_b - i_{b,l}|)$, should be specified based on the performance and design requirements of a specific HESS.

$$a = \frac{1}{(i_{b,max} - i_{b,ave})^2} \tag{13}$$

$$b = \frac{1}{[Max(|i_b - i_{b,l}|)]^2} \tag{14}$$

Meanwhile, the utility function of the UC pack u_c can be represented as an utility of its stored energy $u_{c,eng}$ with a weight coefficient $w_{c,eng}$:

$$u_c = w_{c,eng}[1 - c(i_c - i_{c,fit})^2], \tag{15}$$

where

$$c = \frac{1}{(I_{c,max} - i_{c,fit})^2}. \tag{16}$$

c is calculated in the same way as a and b in Eqs. (13) and (14). $I_{c,max}$ is the maximum permissible current of the UC pack. Considering the equal chance of charging and discharging of an UC pack in a dynamic environment, the UC pack's initial voltage $V_{c,ini}$ could be specified as

$$V_{c,ini} = \sqrt{\frac{V_{c,max}^2 + V_{c,min}^2}{2}}, \tag{17}$$

where $V_{c,max}$ and $V_{c,min}$ are the maximum and minimum voltages of the UC pack, respectively. Thus to control the voltage of the UC pack, its reference current $i_{c,fit}$ is designed by scaling $I_{c,max}$ based on the energy difference between the present and initial levels:

$$i_{c,fit} = \left(2\frac{v_c^2 - V_{c,min}^2}{V_{c,max}^2 - V_{c,min}^2} - 1\right) I_{c,max}. \tag{18}$$

In this way, when i_c is closer to $i_{c,fit}$, the UC pack is properly charged/discharged to reach its initial level of the stored energy.

The utility functions of the battery and UC packs can then be directly used as objective functions (OBJ) of the optimization problem that should be optimized simultaneously,

$$\text{OBJ}_1 : f_{min} = -u_b, \tag{19}$$
$$\text{OBJ}_2 : f_{min} = -u_c. \tag{20}$$

In order to transform this multi-objective optimization problem into a single-objective optimization problem, the weighted-sum method is used. Here the weight-sum method is chosen because it can provide one analytical solution, instead of numerical or heuristic ones, for the following real-time implementation. The entire objective function can be formulated as follows,

$$\text{OBJ} : f_{min} = -w_{b,ave}u_{b,ave} - w_{b,dif}u_{b,dif} - w_{c,eng}u_c, \tag{21}$$

subject to

$$0 \leq (b, w_{ave}, w_{b,dif}, w_{c,eng}) \quad \leq 1, \tag{22}$$

where $w_{b,ave}$, $w_{b,dif}$, and $w_{c,eng}$ are three weight coefficients for the respective utility functions. Other constraints are also necessary to make this optimization problem practically feasible. One important constraint is to guarantee that the sum of the currents from the battery and UC packs is equal to the

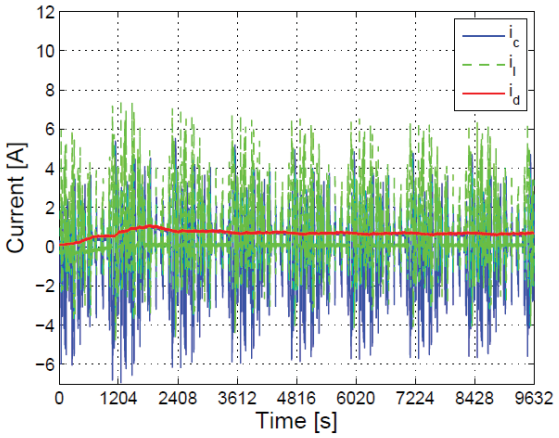

Fig. 8. Overall current responses in experiments.

load current l_l, i.e.,

$$i_c + i_b(1-D) - i_l = 0 \tag{23}$$

where D is the duty cycle of the boost DC-DC converter.

Two design variables of the optimization problem are $x_1 = i_b$ and $x_2 = i_c$. The optimization problem can then be formulated as follows,

$$\begin{aligned} \text{Minimize } f(x_1,x_2) = &- w_{b,ave}[1 - a(x_1 - i_{b,ave})^2] \\ &- w_{b,dif}[1 - b(x_1 - i_{b,l})^2] \\ &- w_{c,eng}[1 - c(x_2 - i_{c,fit})^2] \end{aligned} \tag{24}$$

subject to

$$x_2 + x_1(1-D) - i_l = 0, \tag{25}$$

$$w_{b,ave} + w_{b,dif} + w_{c,eng} = 1, \tag{26}$$

$$0 \le (w_{b,ave}, w_{b,dif}, w_{c,eng}) \le 1. \tag{27}$$

The Karush-Kuhn-Tucker (KKT) conditions are used here to solve the above nonlinear optimization problem theoretically [20], [21]. As long as the values of the weight coefficients are determined, the optimal solution can be updated at each control instant. The coefficients should be determined as the values that can provide the best balance between the different preferences of the battery and UC packs, i.e., the knee point of the Pareto set under a targeted test cycle such as JC08 driving cycle (the Japanese urban test cycle representing congested city driving conditions) [22]–[24]. Figure 8 shows the experimental results for the current of the DC-DC converter, i_d, the current of the UC pack, i_c, and the load current, i_l. It shows that the current of the battery pack (through the DC-DC converter) covers the average load current, the UC pack covers the dynamic current, and the sum of them is the load current.

V. Optimal Load-based Wireless Charging

For the energy storage through the wireless power transfer, ultracapacitors could be more suitable than batteries due to their excellent characteristics. However, an ultracapacitor presents a changing impedance to the whole system during the charging process, which means a fixed design of impedance matching network may not function at its designed performance as the load is changing over time. For a MHz WPT system, its system efficiency (from power amplifier to the final load, UC pack here) relates to the load seen by the rectifier [see Figs. 9 and 10].

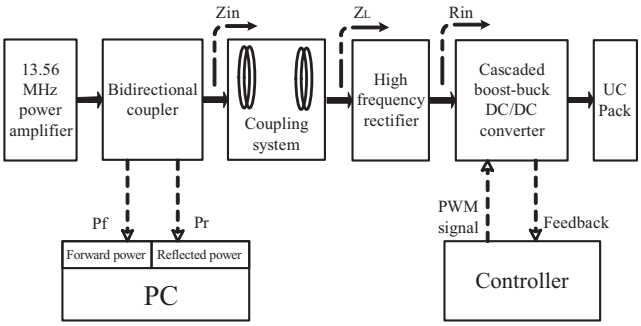

Fig. 9. The configuration of the 13.56MHz wireless power transfer system.

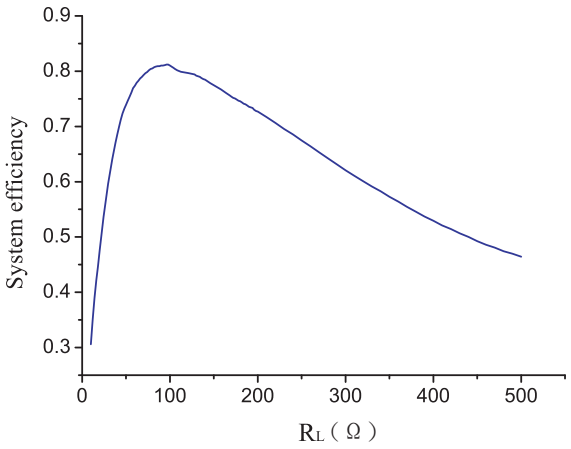

Fig. 10. System efficiency versus load resistance.

As shown in Figs. 9 and Fig. 11, a cascaded boost-buck DC/DC converter can be applied to implement the control of the load seen by the rectifier, provide an optimal load and thus maintain a high overall system efficiency [25]. Taking the buck converter as an example, assume there is no power loss, then

$$\frac{V_{in}^2}{R_{in}} = \frac{V_{out}^2}{R_L}, \tag{28}$$

where V_{in} and V_{out} are the input and output voltages, respectively. R_{in} is input resistance, i.e., the load resistance seen by the rectifier, and here R_L is the load resistance. Since

$$V_{out} = DV_{in}, \tag{29}$$

where D is the duty cycle between 0 and 1, then

$$R_{in} = \frac{R_L}{D^2}. \tag{30}$$

Therefore, the buck converter can realize an equivalent resistance between the real final load resistance, R_L, and $+\infty$. Similarly, the boost converter provides an equivalent resistance from 0 to R_L. By a cascaded connection of the boost and buck converter, any equivalent load resistance between 0 to $+\infty$ can be matched. The circuit board of the cascaded boost-buck converter is shown in Fig. 12. The converter was designed and fabricated in house. The switching frequency of the DC-DC converter is 20 kHz and its dimension is 220 mm$\times$160 mm. The overall efficiency of the DC-DC converter is about 90% assuming a fixed load.

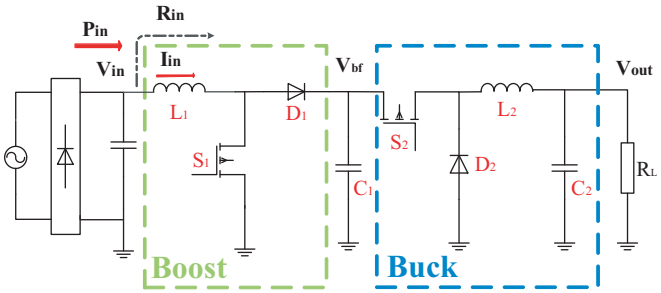

Fig. 11. Cascaded boost-buck converter topology.

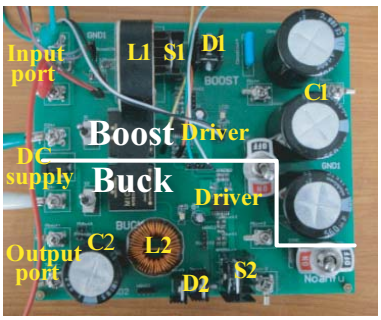

Fig. 12. Cascaded boost-buck converter.

One of the possible control configurations for the cascaded DC/DC converter is illustrated in Fig. 13. Input current I_{in}, input voltage V_{in} and buffer capacitor voltage V_{bf} are the three feedback signals for the control of D_1 and D_2, the duty cycles for the boost and buck converters, respectively [refer to Fig. 11]. The two PI controllers control the equivalent load resistance R_{in} and the buffer capacitor voltage V_{bf}, respectively. The upper PI controller minimizes control error $R_{in}^* I_{in} - V_{in}$, where R_{in}^* is the optimal load resistance seen by the rectifier. The lower PI controller regulates V_{bf} to be equal with kV_{in}, where k is greater than one due to the functionality of the buck converter.

The testing wireless power transfer system is shown in Fig. 14, which consists of a 13.56 MHz class-D PA, a bidirectional coupler for the sensing of forward and reflected power (P_f and P_r), two resonance coils, a rectifier using SiC Schottky diodes, a boost-buck DC-DC converter for impedance matching and an ultracapacitor bank. The specifications for

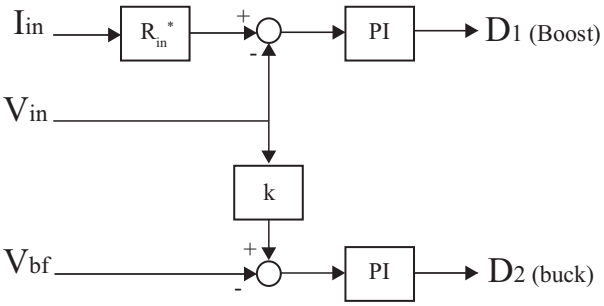

Fig. 13. Duty cycle control blockdiagram for the variable load mode.

TABLE I
ULTRACAPACITOR BANK

Single cell capacitance [F]	700
Single cell maximum voltage [V]	2.7
Number of cells	10
Connection of cells	Serial

the ultracapacitor bank are listed in Tbl. I. In experiments, the duty cycle control is implemented using TI DSP 28335. P_f and P_r can be directly measured by the bidirectional coupler and two power sensors. The load power P_l is determined by the measurement of voltage and current on the load. A general purpose class-D power amplifier is used as the PA with an efficiency of about 80%. 40 Watts forward power from the power amplifier is chosen to demonstrate a medium power transfer capability. The system efficiency here is the ratio of the power received by the ultracapacitor bank, P_l and the forward power P_f from the PA, i.e.

$$\eta = \frac{P_l}{P_f}. \tag{31}$$

As mentioned above, the electrical impedance of the ultracapacitor bank changes over time during the charging period. This dynamic loading to the WPT system can cause a degradation of the system efficiency if no proper circuit is implemented. The proposed cascaded boost-buck DC-DC converter can automatically adjust its duty ratio for optimal system efficiency when charging the ultracapacitor bank. In Fig. 15 (the experimental results), the ultracapacitor's charging status over time is plotted with and without the cascaded boost-buck DC-DC converter. It shows that using the DC-DC converter can improve the system efficiency from 28.1% to 71.5% when charging the ultracapacitor bank.

VI. Conclusion

It is theoretically proved that ultracapacitors work best with dynamic loads and the low-cost batteries designed to provide an average current. And the control of the battery-ultracapacitor HESS is a multi-objective/distributed control problem that can be solved using a utility-function/agent-based approach. Finally, high efficient wireless charging of ultracapacitors needs delicate control due to their largely

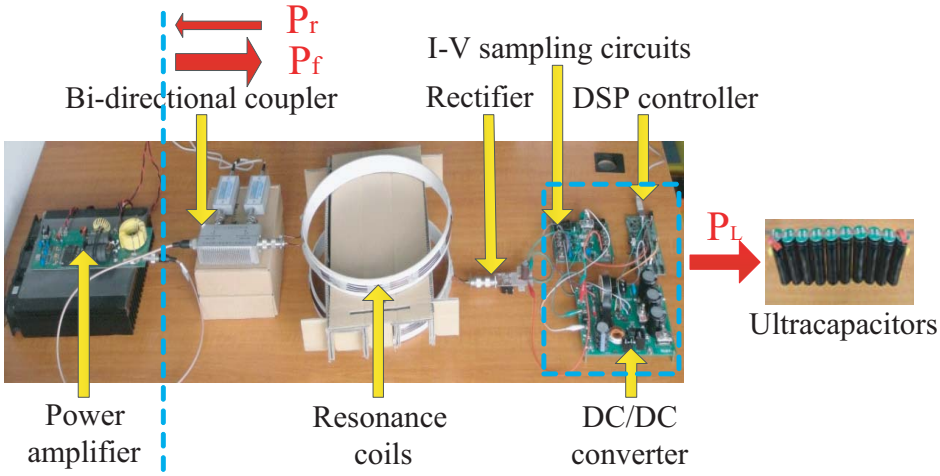

Fig. 14. The testing wireless power transfer system with various loads.

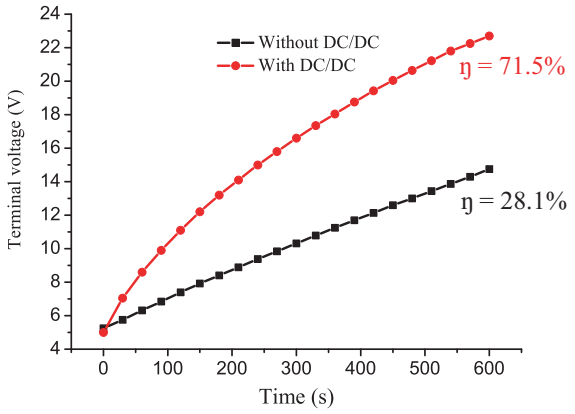

Fig. 15. Ultracapacitors charging improvement using the cascaded boost-buck DC-DC converter.

varying impedance during charging.

ACKNOWLEDGMENT

The authors would like to thank National Science Foundation of China [grant number 509501103 41] and Nippon Chemi-con Ltd., for supporting this work.

REFERENCES

[1] P. Sharma and T. Bhatti, "A review on electrochemical double-layer capacitors," *Energy Convers. Manage.*, vol. 51, no. 12, pp. 2901–2912, 2010.

[2] R. Kötz and M. Carlen, "Principles and applications of electrochemical capacitors," *Electrochim. Acta*, vol. 45, no. 15, pp. 2483–2498, 2000.

[3] A. Khaligh and Z. Li, "Battery, ultracapacitor, fuel cell, and hybrid energy storage systems for electric, hybrid electric, fuel cell, and plug-in hybrid electric vehicles: State of the art," *IEEE Trans. Veh. Technol.*, vol. 59, pp. 2806–2814, Jul. 2010.

[4] J. Cao and A. Emadi, "A new battery/ultracapacitor hybrid energy storage system for electric, hybrid, and plug-in hybrid electric vehicles," *IEEE Trans. Power Electron.*, vol. 27, no. 1, pp. 122–132, 2012.

[5] A. Burke and M. Miller, "The power capability of ultracapacitors and lithium batteries for electric and hybrid vehicle applications," *Journal of Power Sources*, vol. 196, no. 1, pp. 514–522, 2011.

[6] A. Burke, "Ultracapacitors: why, how, and where is the technology," *Journal of Power Sources*, vol. 91, no. 1, pp. 37–50, 2000.

[7] A. Kuperman and I. Aharon, "Battery–ultracapacitor hybrids for pulsed current loads: A review," *Renew. Sust. Energy. Rev.*, vol. 15, no. 2, pp. 981–992, 2011.

[8] J. Moreno, M. E. Ortúzar, and J. W. Dixon, "Energy-management system for a hybrid electric vehicle, using ultracapacitors and neural networks," *IEEE Trans. Ind. Electron.*, vol. 53, no. 2, pp. 614–623, 2006.

[9] X. Zhang, C. C. Mi, A. Masrur, and D. Daniszewski, "Wavelet-transform-based power management of hybrid vehicles with multiple on-board energy sources including fuel cell, battery and ultracapacitor," *J. Power Sources*, vol. 185, no. 2, pp. 1533–1543, 2008.

[10] O. Erdinc, B. Vural, and M. Uzunoglu, "A wavelet-fuzzy logic based energy management strategy for a fuel cell/battery/ultra-capacitor hybrid vehicular power system," *Journal of Power Sources*, vol. 194, no. 1, pp. 369–380, 2009.

[11] M. Zandi, A. Payman, J.-P. Martin, S. Pierfederici, B. Davat, and F. Meibody-Tabar, "Energy management of a fuel cell/supercapacitor/battery power source for electric vehicular applications," *IEEE Trans. Veh. Technol.*, vol. 60, no. 2, pp. 433–443, 2011.

[12] D. Rotenberg, A. Vahidi, and I. Kolmanovsky, "Ultracapacitor assisted powertrains: Modeling, control, sizing, and the impact on fuel economy," *IEEE Trans. Control Syst. Technol.*, vol. 19, no. 3, pp. 576–589, 2011.

[13] O. Laldin, M. Moshirvaziri, and O. Trescases, "Predictive algorithm for optimizing power flow in hybrid ultracapacitor/battery storage systems for light electric vehicles," *IEEE Trans. Power Electron.*, vol. 28, no. 8, pp. 3882–3895, 2013.

[14] M.-E. Choi, S.-W. Kim, and S.-W. Seo, "Energy management optimization in a battery/supercapacitor hybrid energy storage system," *IEEE Trans. Smart Grid*, vol. 3, no. 1, pp. 463–472, 2012.

[15] J. Fishelson, K. Heaslip, W. Louisell, and K. Womack, "An evaluation framework for an automated electric transportation network," in *Proc. The 90th Transportation Research Board Annual Meeting*, Washington DC, Jan. 2011.

[16] H. Rakouth, J. Absmeier, A. Brown Jr, I.-S. Suh, R. Sumner, R. Henderson *et al.*, "EV charging through wireless power transfer: Analysis of efficiency optimization and technology trends," in *Proc. The FISITA 2012 World Automotive Congress*, Beijing, China, Nov. 2013, pp. 871–884.

[17] A. Kuperman, I. Aharon, S. Malki, and A. Kara, "Design of a semi-active battery-ultracapacitor hybrid energy source," *IEEE Trans. Power Electron.*, vol. 28, no. 2, pp. 806–815, 2013.

[18] L. Wang, E. G. Collins, and H. Li, "Optimal design and real-time control for energy management in electric vehicles," *IEEE Trans. Veh. Technol*, vol. 60, pp. 1419–1429, May 2011.

[19] H. Yin, C. Zhao, M. Li, and C. Ma, "Optimization based energy control for battery/super-capacitor hybrid energy storage systems," in *Proc. IEEE Industrial Electronics Society, (IECON'2013)*, Vienna, Austria, Nov. 2013, pp. 6764–6769.

[20] J. Arora, *Introduction to optimum design*. Academic Press, 2004.
[21] N. Rahbari-Asr and M. Chow, "Cooperative distributed demand management for community charging of PHEV/PEVs based on KKT conditions and consensus networks," in *IEEE Trans. Ind. Informat. to be published*, vol. PP, no. 99, 2014, pp. 1–1.
[22] J. Branke, K. Deb, H. Dierolf, and M. Osswald, "Finding knees in multi-objective optimization," in *Parallel Problem Solving from Nature-PPSN VIII*. Springer, 2004, pp. 722–731.
[23] K. Kiyota, H. Sugimoto, and A. Chiba, "Comparison of energy consumption of SRM and IPMSM in automotive driving schedules," in *Proc. IEEE Energy Conversion Congress and Exposition (ECCE'12)*, Raleigh, NC, USA, Sep. 2012, pp. 853–860.
[24] S. Chopra and P. Bauer, "Driving range extension of EV with on-road contactless power transfer-a case study," *IEEE Trans. Ind. Electron.*, vol. 60, no. 1, pp. 329–338, 2013.
[25] M. Fu, C. Ma, and X. Zhu, "A cascaded boost-buck converter for high efficiency wireless power transfer systems," *IEEE Trans. Ind. Informat.*, vol. 10, no. 3, pp. 1972–1980, 2014.